Optical Materials 140 (2023) 113896

Contents lists available at ScienceDirect

Optical Materials

journal homepage: www.elsevier.com/locate/optmat

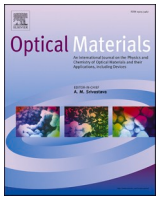

Research Article

Role of the thermal treatment on the microstructure of YAGG nanopowders prepared by urea glass route

Francesco Armetta [a,b], Mattia Gaboardi [c,d,**], Jasper Plaisier [e], Maria Luisa Saladino [a,b,*]

[a] Dipartimento Scienze e Tecnologie Biologiche, Chimiche e Farmaceutiche – STEBICEF, Università degli Studi di Palermo, Parco d'Orleans II, Viale delle Scienze pad. 17, I-90128, Palermo, Italy
[b] IPCF-CNR, Istituto per i Processi Chimico Fisici, V.le F. S. d'Alcontres 37, I-98158, Messina, Italy
[c] Chemistry Department, University of Pavia and C.S.G.I., Viale Taramelli, 16, 27100, Pavia, Italy
[d] Materials Physics Center, CSIC-UPV/EHU, Paseo Manuel de Lardizabal 5, 20018, Donostia - San Sebastian, Spain
[e] Elettra-Sincrotrone Trieste S.C.p.A., Strada Statale 14 - km 163.5, AREA Science Park, 34149, Basovizza, Trieste, Italy

ARTICLE INFO

Keywords:
YAGG phosphors
Rare-earth ions
Urea glass route
X-ray diffraction
Phase evolution

ABSTRACT

Yttrium aluminium gallium garnet (YAGG, $Y_3Al_2Ga_3O_{12}$) doped with rare-earth ions has drawn large attention owing to its optical properties with applications ranging from persistent luminescent phosphors to nanothermometers. Herein, three different YAGG materials were synthesized via the urea glass route followed by thermal treatment, relatively undoped; doped with Ce^{3+}, Cr^{3+}, and Nd^{3+}; and doped with Ce^{3+}, Cr^{3+}, and Yb^{3+}. The garnet formation was studied *in situ* upon thermal treatment from 300 to 1000 °C using synchrotron powder diffraction. Our results show that with this method, the onset of formation of the garnet is about 860 °C, with comparable cell parameters for both undoped and doped YAGG. A possible growth mechanism of YAGG is therefore discussed on the basis of observed microstructural parameters such as occupancy, microstrain, and crystallite size.

1. Introduction

Yttrium Aluminum Gallium Garnet (also known as YAGG or $Y_3Al_2Ga_3O_{12}$), the cubic structure of which is described in the space group $Ia\bar{3}d$, is commonly doped with rare-earth metal ions, granting it peculiar luminescent properties and drawing applications such as persistent luminescent materials, nanothermometers and sensors. Polycrystalline YAGG, co-doped with several lanthanide ions, has been intensively studied by Tanabe et al. [1–6].

However, the interest of researchers is still growing since the optical properties of these crystals and nanocrystals, as well as their applications, depend on the doping element and synthesis route that may influence particle size distribution and morphology, as well as the distribution of defects at the microscopic scale. Special attention has been given to the investigation of the mechanism involved in the phenomena of persistent luminescence (PersL) [7,8] and to nanothermometry [9], both correlated to the particular size and aggregation of particles or lattice defects [10]. Recently, we reported on the particle size-related limitations of persistent phosphors based on nanocrystalline YAGG obtained via Pechini's method [11], co-precipitation [12], and urea glass route (UGR) [13,14]. Although at higher annealing temperatures the properties of the resulting phosphors do not display significant changes, the smallest crystallites exhibit an increased number of surface defects leading to PersL quenching [15,16].

The UGR is a one-pot green and inexpensive method leading to high yields and therefore suitable for large-scale production. Following this procedure, metallic salts are solubilized in ethanol and after the addition of urea, they form a so-called *gel-like* phase [13,17]. This starting material is directly treated, in air, at high temperature (>900 °C) inside a furnace to finally obtain the garnet. Urea in ethanol can form complexes with many metals, usually through the carbonyl group or, in the case of softer metals, with the nitrogen atoms of the amino groups. The gel-like phase is the result of the ability of urea to form a polymeric framework, able to accommodate the nuclei that will grow during the subsequent heat treatment. During the thermal treatment, alongside with matrix decomposition, the nuclei form crystalline nanoparticles. However, the

* Corresponding author. Dipartimento Scienze e Tecnologie Biologiche, Chimiche e Farmaceutiche – STEBICEF, Università degli Studi di Palermo, Parco d'Orleans II, Viale delle Scienze pad. 17, I-90128, Palermo, Italy.
** Corresponding author. Chemistry Department, University of Pavia and C.S.G.I., Viale Taramelli, 16, 27100 Pavia, Italy.
E-mail addresses: m.gaboardi86@gmail.com (M. Gaboardi), marialuisa.saladino@unipa.it (M.L. Saladino).

https://doi.org/10.1016/j.optmat.2023.113896
Received 30 March 2023; Received in revised form 6 May 2023; Accepted 10 May 2023
Available online 22 May 2023

ultimate formation of the garnet phase depends on the urea-to-metals ratio and on the temperature of treatment [13,18]. This method enables for the production of non-agglomerated nanoparticles with well-defined shape and smaller size (10–45 nm) compared to those obtained by using other synthetic procedures. The optical properties depend not only on the type of dopant, but also on the temperature of treatment, which influences the chance to show either conventional or persistent luminescence mechanisms.

Since changes in the optical properties are originated both by differences in the conductive band [19,20] and the disordered occupancy of Gallium in the tetrahedral (T_h) or octahedral (O_h) sites of the garnet lattice [19], many authors have studied the structure of YAGG [21]. However, a clear trend in the occupation of these sites has proven rather elusive. Fu et al., investigating a series of powders prepared by solid-state reaction, claim that Ga^{3+} preferably occupies the O_h site and, only when the latter is saturated, it will also enter into the T_h site [21]. Jiang et al., on the other hand, sustain that it is difficult for Ga^{3+} to fill the T_h site when three or more Al^{3+} ions were displaced, which leads to the appearance of impurities, and they prepared YGG observing a lattice expansion increasing with the content of Ga [22]. Park et al. demonstrated that the substitution of Ga^{3+} with Al^{3+} in the $Lu_{2.94}(Al_{1-x}Ga_x)_5O_{12}$:0.06$Ce^{3+}$ phosphor, modifying the O^{2-}–O^{2-} bond distances, reduces the lattice distortion around the Ce^{3+} ions causing a blue shift in the emitted light [23].

Considering the garnet features on influencing the optical properties and bearing in mind the importance of temperature, we herein report the first *in situ* structural study on the formation of the garnet phase by UGR upon thermal treatment using synchrotron X-ray powder diffraction (SXRPD). This information could be useful to better understand whether or not the final garnet structure is correlated to its formation pathway, as already reported for YAG nanoparticles prepared in bicontinuous microemulsion [24].

2. Materials and methods

2.1. Materials

Urea (Acros Organics, 98%), absolute ethanol (Aldrich, 99.98%), $Y(NO_3)_3{\cdot}6H_2O$ (Aldrich, 99.8%), $Al(NO_3)_3{\cdot}9H_2O$ (Aldrich, 98%), $Ga(NO_3)_3{\cdot}9H_2O$ (Aldrich, 99.9%), $Ce(NO_3)_3{\cdot}6H_2O$ (Aldrich, 99.99%), $Cr(NO_3)_3{\cdot}9H_2O$ (Fluka, 97%), $Nd(NO_3)_3{\cdot}6H_2O$ (Sigma-Aldrich, 99.99%) and $Yb(NO_3)_3{\cdot}5H_2O$ (Aldrich, 99.99%).

2.2. Synthesises of YAGG materials

For this work, we synthesized three different samples: a reference phase of undoped $Y_3Al_2Ga_3O_{12}$ (simply referred to as YAGG in the following) and two ternary-doped compositions: both made using Ce^{3+} and Cr^{3+} as common dopants, plus a third element (Yb^{3+} or Nd^{3+}) as extra dopant, as summarized in Table 1.

The synthesis of undoped YAGG ($Y_3Al_2Ga_3O_{12}$) and of the two ternary-doped compositions, respectively with Ce, Cr, and Yb (*i.e.*, $Ce_{0.006}Yb_{0.0075}Cr_{0.0125}Y_{2.9865}Al_{1.9875}Ga_3O_{12}$, hereafter labelled [Yb,Ce,Cr]:YAGG) and with Ce, Cr, and Nd (*i.e.*, $Ce_{0.006}Nd_{0.03}Cr_{0.0126}Y_{2.964}Al_{1.9874}Ga_3O_{12}$, hereafter [Nd,Ce,Cr]:YAGG) were performed following procedures reported elsewhere [14]. A solution in ethanol containing salts in the proper molar ratio was prepared by setting the concentration of $Y(NO_3)_3$ to 0.12 mol L^{-1}. An appropriate amount of urea was added to the ethanolic solution with metals to the following molar ratios, R = urea/metals = 1. The obtained systems were subjected to agitation in an ultrasonic bath for 20 min to obtain homogeneous and transparent dispersions identifiable as the gel-like system. The gel was then treated at 400 °C for 4 h in a furnace to eliminate any trace of organic compounds and shrink the volume to a dry powder. A scheme of the procedure, divided in two steps, is reported in Fig. 1.

Table 1
Labels and chemical compositions of the three samples investigated in this work.

Label	Chemical composition
YAGG	$Y_3Al_2Ga_3O_{12}$
[Yb,Ce,Cr]:YAGG	$Ce_{0.006}Yb_{0.0075}Cr_{0.0125}Y_{2.9865}Al_{1.9875}Ga_3O_{12}$
[Nd,Ce,Cr]:YAGG	$Ce_{0.006}Nd_{0.03}Cr_{0.0126}Y_{2.964}Al_{1.9874}Ga_3O_{12}$

2.3. Synchrotron powder diffraction

Due to the disordered and nanostructured nature of YAGG obtained with this method and the inevitable presence of an abundant amorphous fraction, the use of a synchrotron source was deemed necessary to obtain a fair signal-to-noise ratio, enabling for the determination of crystalline phases that are present in small amounts. An initial test was carried out trying to directly measure the semi-liquid gel upon decomposition and further garnet crystallisation. However, due to the large amount of empty volume probed by the beam and the drifting of the sample away from the exposed area upon decomposition, it was not possible to collect reliable information. For this reason, all gels were calcined at 400 °C before the synchrotron experiment in order to attain a shirked specimen containing enough sample, yet avoiding the decomposition step. Dried gel powders were ground and thus inserted into 0.3 mm thick quartz capillaries. The single capillary was then installed and aligned horizontally on the head of a rotating goniometer stage so that it was halfway inserted into the constant temperature region (an alumina working tube wrapped in resistive wire of 80 mm length and 8 mm internal diameter) of the *in situ* cylindrical furnace [25]. The latter is mounted at the end of the MCX beamline at the Elettra synchrotron light-source (Trieste, Italy) [26]. The base of the capillary was left open and connected externally to the oven through an *o*-ring tight Teflon tube, so as to have a constant reservoir of oxygen for the formation of the garnet phase. Thermal treatments were scripted in setpoints followed by a suitable holding time and followed by fast XRPD scans from 650 to 750 °C (25 °C step, 60 s stabilisation time) and from 760 to 1000 °C (10 °C step, 60 s stabilisation time). In the case of YAGG, the sample was kept at 1000 °C for 2.5 h and measured every 30 min. The temperature is read by a K-type thermocouple positioned at the centre of the working tube and its signal amplified by a MAX-31855 (Digilent). The amplified signal is then converted to a temperature by an Arduino-Uno microcontroller, carrying out a PID routine (library by B. Beauregard [27]) and communicating to the computer. Power control is carried out by the microcontroller via the ON/OFF activation of a 100 V AC-voltage triggered by a solid-state relay. A Matlab script allows to program the thermal ramp and diffraction patterns acquisition. Powder diffraction data were obtained from the integration of the Debye ring intersections impinged onto a translating curved image plate positioned around the furnace and covering the 2 θ range 2–130°. Each pattern is captured by lifting the beam stopper (for 120 s acquisition time) positioned in front of the furnace and by shifting the image plate by 3 mm at each following acquisition. Data were collected after aligning the beamline at 12 keV. A silicon standard (NIST SRM 640c) was refined at room temperature to determine the wavelength (λ = 1.0316 Å) and instrument profile parameters. Rietveld refinements were carried out using the GSAS-II software [28]. A suitable Chebyshev polynomial was employed to simulate the incoherent background fraction (*i.e.* amorphous phase from the quartz capillary and decomposed organic fraction in the sample). To model the extra-broadening observed in most powder patterns both isotropic microstrain and isotropic size analysis were implemented. At the same time, lattice parameters were refined upon temperature variation.

3. Results and discussion

The phase evolution process of the dried-gel treated at various temperatures was followed *in situ* by s-XRPD (Fig. 2). The XRD patterns

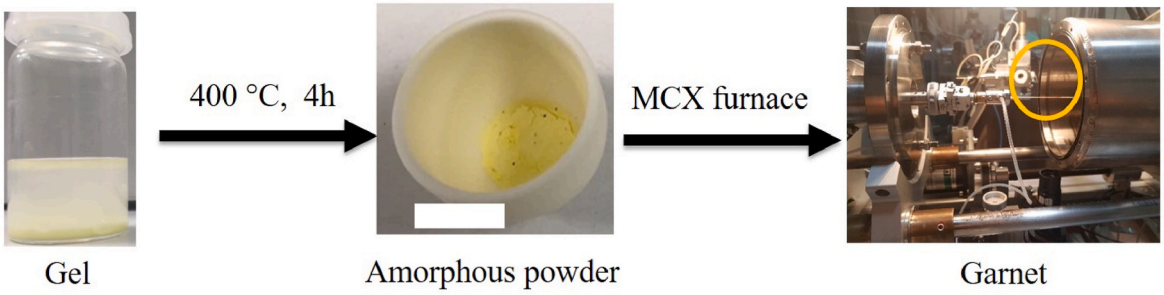

Fig. 1. Scheme of the preparation and investigation of YAGG samples: (1) gel suspension obtained via UGR; (2) specimen obtained after calcination; (3) capillary (orange circle) containing the powder mounted on the open MCX oven in preparation of the *in situ* experiment.

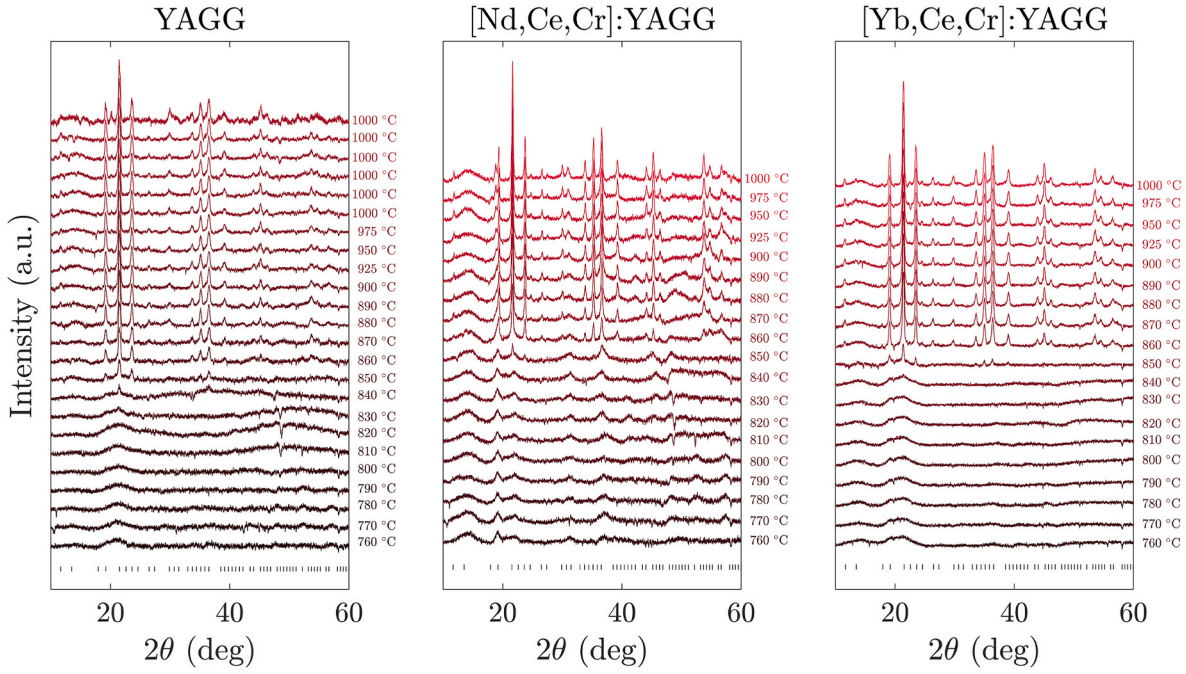

Fig. 2. *in situ* XRPD patterns of YAGG, [Nd,Ce,Cr]:YAGG, and [Yb,Ce,Cr]:YAGG (λ = 1.0316 Å) prepared *via* UGR method and displayed upon formation for the heating range 760–1000 °C. Isotherm scans at 1000 °C in the case of YAGG were also made every 30 min. Vertical tick marks highlight expected reflections for the cubic garnet phase. Displayed data are normalised to the total intensity and rigidly shifted. A suitable background was subtracted to improve contrast and remove the incoherent signal from the capillary.

of the samples calcined at 400 °C display highly amorphous features, with a broad band centred at about 20°, in proximity of the most intense 400, 420, and 422 reflections expected for the cubic phase. Rietveld refinement at this stage is impracticable. Already at 650 °C sample [Nd,Ce,Cr]:YAGG shows more distinct features in this range, however, no apparent changes were observed for this phase at higher temperatures, suggesting the extrinsic origin of these features (that were thus fitted as background). It is worthwhile emphasising that these profiles show slight differences, hinting at an effect of the doping agent on the amorphous organisation.

In the case of un-doped YAGG, the onset of formation of the garnet phase is at about 840 °C, with the appearance of a first weak 420 reflection. For all the samples, the crystalline garnet phase starts growing remarkably at 850 °C. This temperature is slightly lower than that previously reported for garnet formation using the same route [13,14]. Above 850 °C the garnet phase evolves without formation of secondary phases up to 1000 °C. Rietveld refinement was carried out as a function of the temperature, including the analysis of the profile using a model for isotropic domains and microstrain, as expected for a cubic system.

Due to the very low signal-to-noise ratio, some of the patterns were refined by fixing certain parameters (typically occupancy or size, depending on the sample and values) in order to keep the errors at a reasonable level and to avoid undesired correlations, while maintaining a physical sense. Fig. 3 displays the Rietveld refined data for un-doped YAGG at 1000 °C as an example. An increasing background at high angle hints to an effect of fluorescence. Refinements of the other samples at various temperatures display very similar features. The average refined R_{wp} for all patterns was 2.8%, with a standard deviation of 0.5%. The refined occupancies for Ga and Al in the O_h and T_h sites (respectively corresponding to the 16*a* and 24*d* Wyckoff positions) are reported in Fig. 4. In all samples, at the onset of formation of the garnet phase Ga dominates in both sites. However, the diffusion of Al and Ga in the O_h site appears to be facilitated at lower temperatures than that of the tetrahedral one. After an initial situation dominated by Ga in the O_h site at 850 °C, Al progressively converges to the same value. Since variations in the O_h site fluctuated about an average value above 890 °C, the refinement flag for this site was lifted above this temperature and the parameter held at the constant value of about 50% occupancy for both Al and Ga. In contrast, the temperature evolution of the tetrahedral site

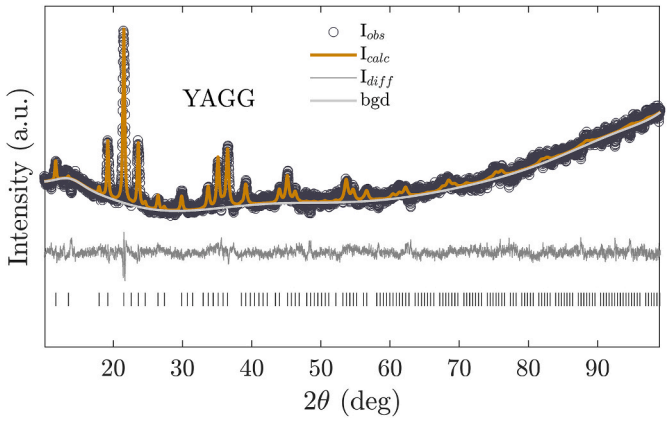

Fig. 3. Rietveld refined XRPD patterns of YAGG at 1000 °C (a = 12.279(2) Å, R_{wp} = 2.6%).

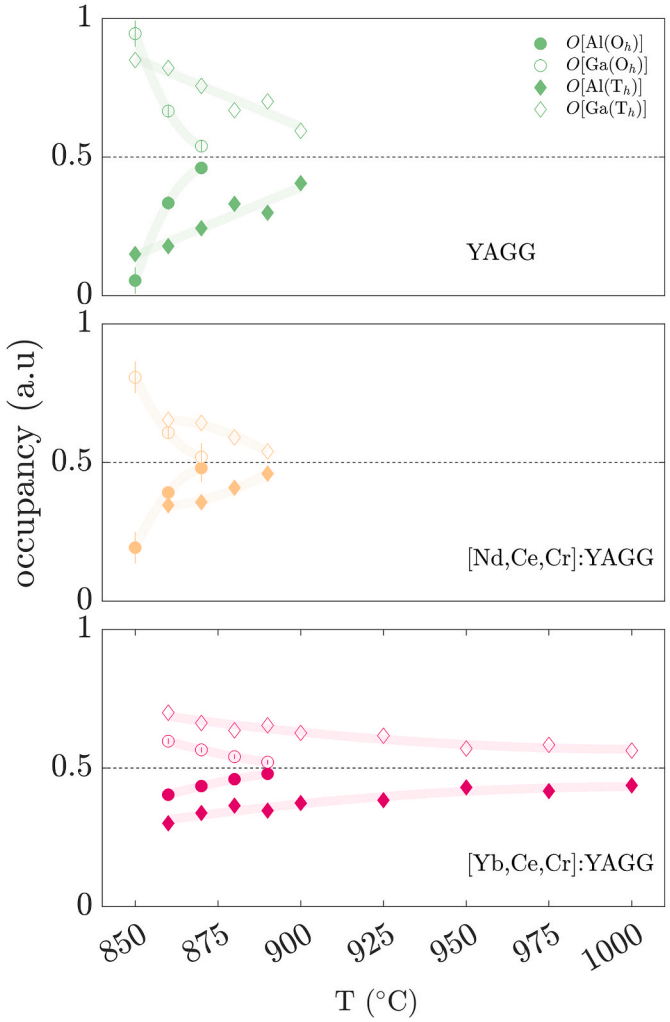

Fig. 4. Rietveld refined occupancies for YAGG, [Nd,Ce,Cr]:YAGG, and [Yb,Ce,Cr]:YAGG reported as a function of the temperature. Filled and empty symbols represent respectively Al and Ga species, while different sites are distinguished by the use of circles (O_h) and diamonds (T_h). Solid lines are a guide to the eye. In the case of non-displayed temperatures, the parameters were kept constant at the last reported value during the refinement.

appears to occur at a lower rate. The best refinement was obtained for [Yb,Ce,Cr]:YAGG, for which the better quality of the data allowed to maintain a good fit of this site up to 1000 °C. For this sample, Ga occupancy in the T_h site (*i.e.* O[Ga(T_h)]) is about 0.7 at 860 °C and slowly decreases to a constant ~0.55 from above 950 °C. In the case of [Nd,Ce,Cr]:YAGG, O[Ga(T_h)] = 0.66 at 860 °C and slowly decreases toward ~0.54 at about 900 °C; while for YAGG, O[Ga(T_h)] changes from ~0.86 at 850 °C to a minimum of about 0.6 at 900 °C. In conclusion, at 1000 °C both sites show approximately balanced fractions of Ga and Al, with an apparent slight excess of Ga in the tetrahedral site. Considering the quality of the XRD patterns, it seems that for the investigated couple of triple dopants, there are no significant differences in the formation path.

As expected, microstrain is rather high during the initial formation of the garnet phase at 850 °C and progressively decreases to a minimum value with the increasing temperature (Fig. 5). Above 875 °C the microstrain parameters can be considered constant for all samples, with a minimum value of $\delta d/d$ = 0.63(2)% for [Yb,Ce,Cr]:YAGG and a maximum of about 1.35(4)% for YAGG.

Since both size and microstrain broadening tend to correlate, the first parameter was refined carefully only for sample [Nd,Ce,Cr]:YAGG, for which correlations were reduced to the minimum owing to a better signal-to-noise ratio at long Q-values. The nanoparticles have an initial size of about 60 nm, they further grow above 890 °C up to about 90 nm at 950 °C, and additionally increase to about 160 nm at 1000 °C, in agreement with our previous studies [13,14]. Concerning the lattice expansion following the formation of crystalline nanoparticles, samples [Nd,Ce,Cr]:YAGG and [Yb,Ce,Cr]:YAGG allow for a comparison, with a linear expansion of $6.4(2)\cdot10^{-3}$ and $5.5(6)\cdot10^{-3}$ Å K^{-1} respectively (Fig. 6). While the values obtained for sample YAGG are in the same range, the large error in the refined parameters (most likely originated by instability of the synchrotron beam during this experiment) does not allow for a reliable comparison and were therefore omitted. In agreement with previous studies [13,14], the cell parameter of the garnet phase increases with the temperature, and the observed differences are ascribed to the two different pairs of triple dopants.

These findings can be discussed on the basis of the results already present in literature. In fact, while both Fu et al. [21] and Jiang et al. [22] report that Ga selectively occupies the O_h site, Laguta et al. demonstrated by ss-NMR investigation that Ga ions preferably occupy the tetrahedral sites of the garnet, whereas Al ions favour the octahedral sites, despite having a smaller ionic radius with respect to that of Ga owing to the stronger covalency of the Ga−O bond compared with Al–O, as well as the need for decreasing the cation−cation repulsive force [19].

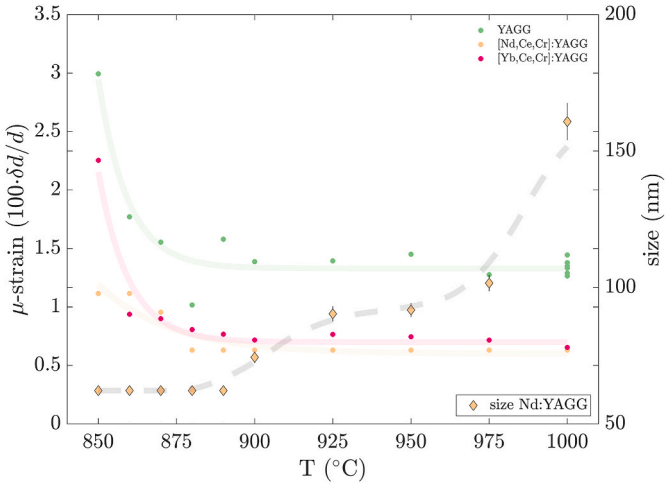

Fig. 5. Rietveld refined isotropic microstrain parameter (left y-axis for YAGG, [Nd,Ce,Cr]:YAGG, and [Yb,Ce,Cr]:YAGG) and size (right y-axis for [Nd,Ce,Cr]:YAGG), reported as a function of the temperature. Solid and dashed lines are a guide to the eye.

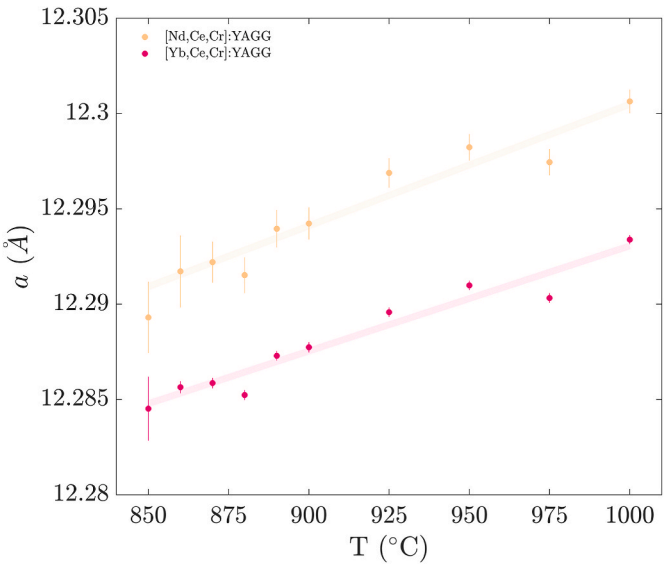

Fig. 6. Rietveld refined lattice parameter as a function of the temperature for [Nd,Ce,Cr]:YAGG and [Yb,Ce,Cr]:YAGG. Solid lines are the linear fit.

On the other hand, for a similar garnet (*i.e.*, $Lu_3Al_{5-x}Ga_xO_{12}$), Yu et al. observed that Ga prefers to fill the tetrahedral sites. In our opinion, these different results could be interpreted by the different preparation methods (solid state rather than precipitation, and so on) and to the various temperature and time of treatment which could ultimately influence the kinetic evolution [29]. In fact, in the above studies, the thermal treatments were performed directly at high temperature and for a long time and the measurements carried out *ex situ*, while, in the present case, the temperature is held for just a few minutes as a result of the *in situ* character of the experiment. On the other hand, even though the gel was treated at 400 °C to remove the organic fraction, we can hardly exclude that some of the by-products may persist in the dried samples and that their presence can influence the formation path of the garnet, creating some interactions between gallium or aluminium and thus decreasing their availability to participate in the crystallisation of YAGG. Similar considerations have been performed in a previous work regarding YAG nanoparticles prepared *via* bi-continuous microemulsion, where the mechanism of formation was explained in terms of an oriented attachment mechanism at low temperature and in terms of Kirkendall effect at high temperature [24].

4. Conclusions

The phase evolution of undoped and ternary-doped YAGG materials, prepared *via* UGR enabled by thermal treatment, has been investigated *in situ* by means of synchrotron X-ray powder diffraction.

A possible growth mechanism of the garnet is discussed based on the observed particle microstructure evolution. From the Rietveld analysis of the XRD patterns, the investigated couple of triple dopants did not show significant difference in the formation path from that of the undoped specimen.

For the undoped YAGG, the onset of formation of the garnet phase is at about 840 °C, while for the doped samples, the crystalline garnet phase starts growing at 850 °C. The crystallite size increases with the temperature, from about 60 to 160 nm. The cell parameter increases linearly with temperature, with an expansion of $6.4(2)\cdot10^{-3}$ and $5.5(6)\cdot10^{-3}$ Å K^{-1} respectively for [Nd,Ce,Cr]:YAGG and [Yb,Ce,Cr]:YAGG.

From the refinement of the two metallic sites, we observed that when the garnet lattice is crystalline (ca. 850 °C), Gallium is occupying both O_h and T_h sites. Based on these results, we can infer that the diffusion of Al and Ga in the octahedral site appears to be facilitated at lower temperatures with respect to the tetrahedral one, with the filling of the latter progressing at a lower rate.

Above 890 °C the O_h site occupancy for both Al and Ga reaches about 50%. At about 1000 °C both sites show approximately balanced fractions of Ga and Al, with an apparent slight excess of Ga in the tetrahedral site.

These findings can be considered as an additional step towards a better understanding of the organisation of Aluminium and Gallium ions in the YAGG lattice, acknowledging that the method of synthesis can influence their distribution in both sites, especially by effect of the temperature and time of treatment.

CRediT authorship contribution statement

Francesco Armetta: Preparation of samples and XRD data collection. **Mattia Gaboardi:** XRD experiment, Formal analysis, instrumentation, Writing – review & editing. **Jasper Plaisier:** Conceptualization, Methodology, Writing – review & editing. **Maria Luisa Saladino:** Conceptualization, Methodology, Writing – review & editing.

Declaration of competing interest

The authors declare that they have no known competing financial interests or personal relationships that could have appeared to influence the work reported in this paper.

Data availability

Data will be made available on request.

Acknowledgments

We are grateful to Elettra-Sincrotrone Trieste for providing beamtime and financial support for the XRPD experiment (proposal nr. 20170489, Role of the thermal treatment on the composition and microstructural evolution of YAG nanoparticles). FA thanks MIUR for the Project 'PON Ricerca e Innovazione 2014–2020 – Avviso DD 407/2018' "AIM Attrazione e Mobilità Internazionale" (AIM1808223). M.G. wishes to thank Alessandro Olivo (Elettra-Sincrotrone Trieste) for the help with the setting and tuning of the Arduino PID and Chiara Milanese (Pavia H2 Lab, Chemistry Department and CSGI - Pavia University) for the support.

References

[1] J. Xu, S. Tanabe, Persistent luminescence instead of phosphorescence: history, mechanism, and perspective, J. Lumin. 205 (2019) 581–620, https://doi.org/10.1016/J.JLUMIN.2018.09.047.

[2] J. Xu, S. Tanabe, A.D. Sontakke, J. Ueda, Near-infrared multi-wavelengths long persistent luminescence of Nd^{3+} ion through persistent energy transfer in Ce^{3+},Cr^{3+} Co-doped $Y_3Al_2Ga_3O_{12}$ for the first and second bio-imaging windows, Appl. Phys. Lett. 107 (8) (2015), 081903, https://doi.org/10.1063/1.4929495.

[3] S. Feng, H. Qin, G. Wu, H. Jiang, J. Zhao, Y. Liu, Z. Luo, J. Qiao, J. Jiang, Spectrum regulation of YAG:Ce transparent ceramics with Pr, Cr doping for white light emitting diodes application, J. Eur. Ceram. Soc. 37 (10) (2017) 3403–3409, https://doi.org/10.1016/j.jeurceramsoc.2017.03.061.

[4] J. Ueda, K. Kuroishi, S. Tanabe, Bright persistent ceramic phosphors of Ce^{3+}-Cr^{3+} Co-doped garnet able to store by blue light, Appl. Phys. Lett. 104 (10) (2014), 101904, https://doi.org/10.1063/1.4868138.

[5] J. Xu, J. Ueda, K. Kuroishi, S. Tanabe, Fabrication of Ce^{3+}–Cr^{3+} Co-doped yttrium aluminium gallium garnet transparent ceramic phosphors with super long persistent luminescence, Scripta Mater. 102 (2015) 47–50, https://doi.org/10.1016/J.SCRIPTAMAT.2015.01.029.

[6] J. Ueda, P. Dorenbos, A.J.J. Bos, K. Kuroishi, S. Tanabe, Control of electron transfer between Ce^{3+} and Cr^{3+} in the $Y_3Al_{5-x}Ga_xO_{12}$ host via conduction band engineering, J. Mater. Chem. C 3 (22) (2015) 5642–5651, https://doi.org/10.1039/C5TC00546A.

[7] D. Chen, Y. Zhou, W. Xu, J. Zhong, P. Huang, Persistent and photo-stimulated luminescence in Ce^{3+}/Cr^{3+} activated $Y_3Al_2Ga_3O_{12}$ phosphors and transparent phosphor-in-glass, J. Mater. Chem. C 4 (48) (2016) 11457–11464, https://doi.org/10.1039/C6TC04140J.

[8] J. Ueda, M. Katayama, K. Asami, J. Xu, Y. Inada, S. Tanabe, Evidence of valence state change of Ce^{3+} and Cr^{3+} during UV charging process in $Y_3Al_2Ga_3O_{12}$

persistent phosphors, Opt. Mater. Express 7 (7) (2017) 2471, https://doi.org/10.1364/OME.7.002471.
[9] P. Bolek, J. Zeler, C.D.S. Brites, J. Trojan-Piegza, L. Carlos, E. Zych, Ga-modified YAG:Pr^{3+} dual-mode tunable luminescence thermometers, Chem. Eng. J. 421 (2021), 129764, https://doi.org/10.1016/j.cej.2021.129764.
[10] F. Armetta, M.A. Sibeko, A.S. Luyt, D.F. Chillura Martino, A. Spinella, M. L. Saladino, Influence of the Ce:YAG amount on structure and optical properties of Ce:YAG-PMMA composites for white LED, Z. Phys. Chem. 230 (9) (2016) 1219–1231, https://doi.org/10.1515/zpch-2015-0703.
[11] Z. Dai, V. Boiko, M. Markowska, A. Gerus, K. Grzeszkiewicz, J. Hölsä, M. L. Saladino, D. Hreniak, Optical studies of $Y_3(Al,Ga)_5O_{12}$:Ce^{3+},Cr^{3+},Nd^{3+} nano-phosphors obtained by Pechini method, Journal of rare earth 37 (2019) 1132–1136.
[12] V. Boiko, M. Markowska, L. Consentino, M.L. Saladino, D. Hreniak, Effect of Ce^{3+} concentration on optical properties including persistent luminescence of YAG:Ce^{3+},Cr^{3+},Nd^{3+} nanophosphors obtained by the co-precipitation method, Opt. Mater. 107 (2020), 109956.
[13] F. Armetta, C. Giordano, C. Defilippi, Ł. Marciniak, D. Hreniak, E. Caponetti, M. L. Saladino, Non-conventional Ce: YAG nanostructures via urea complexes, Sci. Rep. 9 (2019) 3368.
[14] V. Boiko, M.L. Saladino, F. Armetta, F. Ursi, M. Markowska, K. Grzeszkiewicz, C. Mortalò, C. Leonelli, D. Hreniak, Urea-glass route as a way to optimize $Y_3Al_2Ga_3O_{12}$:Ce^{3+},Cr^{3+},Pr^{3+} nanocrystals for persistent luminescence applications, Langmuir 38 (2022) 11539–11549.
[15] V. Boiko, Z. Dai, M. Markowska, C. Leonelli, C. Mortalò, F. Armetta, F. Ursi, G. Nasillo, M.L. Saladino, D. Hreniak, Particle size-related limitations of persistent phosphors based on the doped $Y_3Al_2Ga_3O_{12}$ system, Sci. Rep. 11 (2021) 141.
[16] Z. Dai, V. Boiko, K. Grzeszkiewicz, M. Markowska, J. Hölsä, F. Ursi, M.L. Saladino, D. Hreniak, Effect of annealing temperature on the persistent luminescence of $Y_3Al_2Ga_3O_{12}$:Cr^{3+} co-doped with Ce^{3+} and Pr^{3+}, Opt. Mater. 111 (2021), 110522.
[17] F. Armetta, C. Defilippi, C. Giordano, E. Caponetti, Ł. Marciniak, D. Hreniak, M. L. Saladino, Influence of cerium content and heat treatment on Ce:YAG@glass wool nanostructures, J. Nanoparticle Res. 21 (2019) 152–161.
[18] W. Lei, M.G. Willinger, M. Antonietti, C. Giordano, Chem. Eur J. 21 (2015) 18976–18982.
[19] V. Laguta, Y. Zorenko, V. Gorbenko, A. Iskaliyeva, Y. Zagorodniy, O. Sidletskiy, P. Bilski, A. Twardak, M. Nikl, Aluminum and gallium substitution in yttrium and lutetium aluminum–gallium garnets: investigation by single-crystal NMR and TSL methods, J. Phys. Chem. C 120 (42) (2016) 24400–24408, https://doi.org/10.1021/acs.jpcc.6b08593.
[20] F. Di Quarto, A. Zaffora, F. Di Franco, M. Monica Santamaria, Band gap modeling of different ternary and quaternary alumina garnet phases $Y_3(Al_xGa_{1-x})_5O_{12}$ (YAGG) and $Lu_3(Al_xGa_{1-x})_5O_{12}$ (LuAGG). A semiempirical approach, J. Phys. Chem. C 126 (2022) 17313–17327, https://doi.org/10.1021/acs.jpcc.2c04523.
[21] S. Fu, J. Tan, X. Bai, S. Yang, L. You, Z. Du, Effect of Al/Ga substitution on the structural and luminescence, properties of $Y_3(Al_{1-x}Ga_x)_5O_{12}$: Ce3þ phosphors, Opt. Mater. 75 (2018) 619–625, https://doi.org/10.1016/j.optmat.2017.11.021.
[22] L. Jiang, X. Zhang, S. Zhu, H. Tang, Q. Li, W. Zhang, X. Mi, L. Lu H. Liu, X. Liu, Preparation and luminescence properties of $Y_{3-y}Al_{5-x}Ga_xO_{12}$:$Ce^{3+y}$ phosphors, J. Mater. Sci. Mater. Electron. 29 (2018) 9045–9051, https://doi.org/10.1007/s10854-018-8930-6.
[23] K. Park, H. Kim, G.W. Jung, D.H. Kim, S.Y. Gwon, Development of a correlation between lattice distortion factors and emission wavelengths in Ga–substituted $Lu_3(Al_{1-x}Ga_x)_5O_{12}$:$Ce^{3+}$ ($0 \leq x \leq 0.5$) phosphors, J. Alloys Compd. 921 (2022), 166019, https://doi.org/10.1016/j.jallcom.2022.166019.
[24] F. Armetta, M.L. Saladino, D. Chillura Martino, P. Livreri, M. Berrettoni, E. Caponetti, Synthesis of Yttrium Aluminum Garnet nanoparticles in confined environment II: role of the thermal treatment on the composition and microstructural evolution, J. Alloys Compd. 719 (2017) 264–270.
[25] P. Riello, A. Lausi, J. Macleod, J.R. Plaisier, G. Zerauschek, P. Fornasiero, In situ reaction furnace for real-time XRD studies, J. Synchrotron Radiat. 20 (2013) 194–196, https://doi.org/10.1107/S0909049512039246.
[26] L. Rebuffi, J.R. Plaisier, M. Abdellatief, A. Lausi, P. Scardi, MCX: a synchrotron radiation beamline for X-ray diffraction line profile analysis, J. of Inor. And General Chem. . 640 (15) (2014) 3100–3106, https://doi.org/10.1002/zaac.201400163.
[27] https://github.com/br3ttb/Arduino-PID-Library.
[28] B.H. Toby, R.B. Von Dreeledoi, GSAS-II: the genesis of a modern open-source all purpose crystallography software package, J. Appl. Crystallogr. 46 (2013) 544–549, https://doi.org/10.1107/S0021889813003531.
[29] O. Yu V. Zagorodniy, H. Chlana, Y. Štěpánková, J. Fomichov, V.V. Pejchal, M. Laguta, Gallium preference for the occupation of tetrahedral sites in $Lu_3(Al_{5-x}Ga_x)O_{12}$ multicomponent garnet scintillators according to solid-state nuclear magnetic resonance and density functional theory calculations, J. Phys. Chem. Solid. 126 (2019) 93–104, https://doi.org/10.1016/j.jpcs.2018.10.027.